

Finite Element Analysis of Drilling of Carbon Fibre Reinforced Composites

Ozden Isbilir · Elaheh Ghassemieh

Received: 29 April 2011 / Accepted: 4 August 2011 / Published online: 18 August 2011
© Springer Science+Business Media B.V. 2011

Abstract Despite the increased applications of the composite materials in aerospace due to their exceptional physical and mechanical properties, the machining of composites remains a challenge. Fibre reinforced laminated composites are prone to different damages during machining process such as delamination, fibre pull-out, microcracks, thermal damages. Optimization of the drilling process parameters can reduce the probability of these damages. In the current research, a 3D finite element (FE) model is developed of the process of drilling in the carbon fibre reinforced composite (CFC). The FE model is used to investigate the effects of cutting speed and feed rate on thrust force, torque and delamination in the drilling of carbon fiber reinforced laminated composite. A mesoscale FE model taking into account of the different oriented plies and interfaces has been proposed to predict different damage modes in the plies and delamination. For validation purposes, experimental drilling tests have been performed and compared to the results of the finite element analysis. Using Matlab a digital image analysis code has been developed to assess the delamination factor produced in CFC as a result of drilling.

Keywords Carbon fibres reinforced composites · Polymer matrix composites · Delamination · Finite element analysis · Drilling · Cohesive zone

Abbreviations

σ	Normal stress
τ	Shear stress
C, K	Stiffness matrix
C_d	Stiffness matrix after damage initiation
D	Damage coefficient
d	Damage variables in any mode
ε	Normal strain
γ	Shear strain

O. Isbilir · E. Ghassemieh (✉)
Mechanical Engineering Department, University of Sheffield, Sir Fredrick Mappin Building, Mappin Street, S1 3JD Sheffield, UK
e-mail: E.Ghassemieh@sheffield.ac.uk

E	Elasticity modulus
G	Shear modulus
ν	Poisson's ratio
d	Density
$\sigma^{f, t}$	Strength of the material in tension in any direction
$\sigma^{f, c}$	Strength of the material in compression in any direction
F_f^C	Hashin's damage initiation criterion in fibre mode in compression
F_f^T	Hashin's damage initiation criterion in fibre mode in tensile
F_M^C	Hashin's damage initiation criterion in matrix in compression
F_M^T	Hashin's damage initiation criterion in matrix in tensile
u	Displacement
u_{eq}^0	Equivalent displacement at the damage initiation
u_{eq}^f	Equivalent failure displacement
G	Energy
G^C	Critical energy
μ	Friction coefficient

1 Introduction

Composite materials are one of the most attractive materials in the industry. Particularly, the use of carbon fibre reinforced plastic (CFRP) composites have increased considerably in aerospace, automotive and transport industries due to their superior properties such as strength/weight ratio [1]. Their light weight and high strength characteristics make them suitable in applications where a high strength-to-weight ratio is desirable such as wings and tails in aero structures.

Although composites components are produced to near-net shape, machining is often needed for the assembly requirements. Among the several machining processes, drilling is one of the most common production methods of holes for rivets and bolts. In spite of their attractive physical and mechanical properties, machining of composite materials is challenging and considerably distinct from cutting homogeneous materials [2]. In metal cutting, the main deformation mechanism is plastic deformation. Whereas in composites, particularly carbon fibre reinforced composites, there is not any plastic deformation in the machining process. Cutting tool enforces the carbon fibres fracturing rather than shearing. Instead of having a chip flow over the cutting edge which is observed in metal cutting, only dusty and abrasive chip is generated in the machining of CFRP. Thus the material removal process can be described as shattering with the chip formation that causes increased abrasion of the cutting tool.

Since the composite material has anisotropic layered structure including very abrasive fibre reinforcement, it is difficult to reach a desirable hole quality and to provide a desirable tool life in drilling. The cutting edges of drills are worn dramatically due to the very abrasive fibres, and the machined surfaces are normally highly deteriorated. In addition, machining of composites can cause several problems in the work piece such as fibre pull-out, matrix softening/melting, stress concentration, microcracking and delamination.

Delamination is one of the most common and serious damages in the drilling of composite materials [3]. It can cause a significant reduction in the performance of the laminated composite structures, so it can often be a limiting factor for structural applications. For instance, delamination induced problems accounts for 60% of all rejections in final assembly in the aircraft industry [4]. Thus it is essential to seek drilling methods to minimise the delamination [5–7]. Several techniques have been developed to

reduce delamination, based on adequate selection of cutting parameters, tool geometry, tool material and the use of back-up plate.

Cutting forces and delamination can be predicted both analytically and numerically. Analytical studies based on linear elastic fracture mechanics (LEFM) theory have predicted the critical cutting forces at the onset of delamination during the drilling of composites. The first analytical model was presented by Hocheng and Dharan [8]. According to this model, if the thrust force exceeds the critical thrust force, delamination will occur. The uncut thickness of the work piece in the hole vicinity has to withstand the indentation force due to the movement of the drill. As the drilling progresses, the critical thrust force drops gradually to zero towards the exit side of the laminate. After Hocheng and Dharan model, several other analytical models have been presented [9–12]. The models assume different material models and force distributions at the work piece/tool contact.

Numerical models are very important in the comprehension and optimization of machining processes. An accurate and reliable simulation enables good predictions in terms of temperature, strain and stress distributions; cutting forces and torque; and delamination by taking into account of the complex tool geometry and process parameters. A complete experimental study on drilling is uneconomic due to high cost. Thus, finite element analysis is required to simulate the drilling process. With the advent of computer aided engineering (CAE) technology and high speed computers, simulation of the drilling process using finite element analysis provides an excellent tool for this tough design demand.

A number of researchers have studied numerical analyses of machining of fibre reinforced composites. Finite element analysis of orthogonal cutting of fibre reinforced composite was proposed by Arula and Ramulu using maximum stress and Tsai-Hill criteria [13]. These researchers have stated that chip formation and material removal is particularly dependent on fibre orientation. Other researchers have proposed the FE analysis of drilling of unidirectional CFRP in 3D to predict cutting force and delamination by simplification to orthogonal model [14, 15]. These researchers developed a model which is based on fracture mechanics and the energy release rates. The model uses virtual crack extension (VCE) method. The model estimates the critical thrust force better than previous analytical model [8]. Some investigations have been performed on delamination and thrust force in the drilling of composite material [16, 17]. Carbon fibre reinforced epoxy laminates with a stacking order [0/-45/90/45]_{4s} were used in the numerical investigation. Instead of a general VCE method, delamination is modelled by the use of cohesive interface elements in the model. A very basic cone shape has been used as indenter in the finite element model which is a static analysis and does not take into account of the mass and inertia effects. The model generally estimates the critical thrust force lower than the analytical models. However, none of the previous analytical and numerical studies above have considered the influences of process parameters and tool geometry on delamination and cutting forces.

In this research study, a 3D finite element (FE) model of the process of drilling in the carbon fibre reinforced composite (CFC) is developed. Constitutive damage models are reviewed and the most representative models are selected for the model. The FE model is used to investigate the effects of cutting speed and feed rate on thrust force, torque and delamination in the drilling of carbon fibre reinforced laminated composite. A mesoscale FE model taking into account of the different oriented plies and interfaces has been proposed to predict different damage modes in the plies and delamination. For validation purposes, experimental drilling tests have been performed and compared to the results of the finite element analysis. Using Matlab a digital image analysis code has been developed to assess the delamination factor produced in CFC as a result of drilling.

2 Methodology

2.1 Finite Element Model

In this study a 3D finite element (FE) model which is based on Lagrangian formulation is developed to simulate the drilling process. Commercial finite element software ABAQUS/Explicit is used. The mass and inertia effects are included in the model. Due to the dynamic characteristics of the process, dynamic explicit finite element integration has been proposed in the study. The model aims to simulate the drilling process, to calculate the damage initiation and evolution in the work piece material; to predict induced cutting forces, torque, stress distribution in the work piece throughout the drilling process; and to predict the delamination at the entrance of the hole. Thermal issues are not accounted for in the model since high amount of coolant is used in the experiments. Details of the FE model are discussed below.

2.1.1 Geometry, Mesh and Elements

A uni-directional (UD) carbon fibre reinforced laminated composite work piece having dimensions of 40 mm×40 mm×4.16 mm consists of 16 plies with a stacking sequence of $[90/-45/0/45]_{2s}$. Each ply has 0.26 mm thickness with particular fibre orientation. To be able to predict the effect of process parameters on drilling of CFC, it is important to have a model that is able to include the real geometry, the material properties and the kinematics of the drill. For this purpose, a complex 3-D drill is modelled and imported into the FE simulation. An 8 mm diameter twist drill with 140° point angle and 45° helix angle geometry is used in the drilling of UD CFRP. Initially, cutting tool is assumed fully elastic material to calculate the mass and inertia in the FE model. Then the drill is modelled as a rigid body; mass and inertia are added to the rigid tool to simulate equivalent kinematics of the process. The use of rigid tool in the FE simulation would decrease computational time and maintain the efficiency of the FE analysis. A similar geometry was used in the drilling tests to able to validate the model. Figure 1 (a) shows the work piece and the drill.

Optimisation of the mesh used in this simulation is not a trivial matter and has been one of the subjects of our research. Considering the very complicated geometry and the need for extremely high computing resources a balance between the high accuracy results and

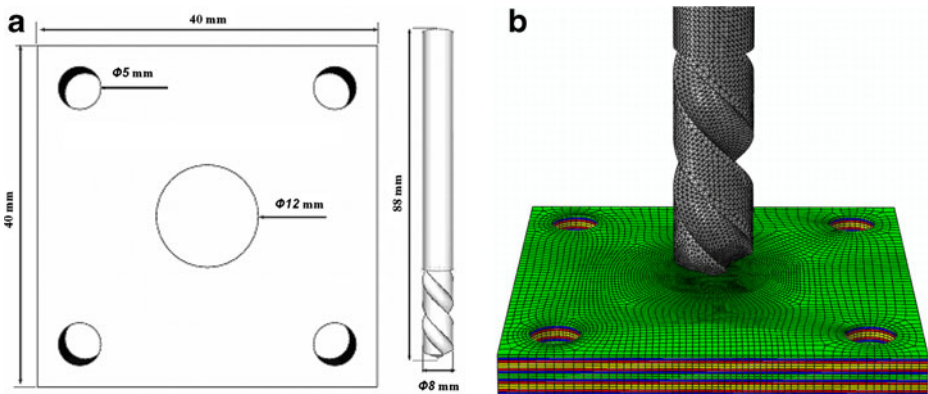


Fig. 1 a Work piece and tool geometry. b The FE model

reasonable element size should be made. The mesh presented here is the mesh that is optimized through a lengthy mesh and conversion study. In order not to deviate from the main objective of our study we have not elaborated on the mesh study here. The mesh size of the work piece is refined in the drilling area and the high stress gradient locus to model the process accurately. The refined region is modelled as cylindrical and elements in this region are removed when the failure criterion has met during the simulation. The laminated work piece is modelled using 8-node continuum shell elements with reduced integration (SC8R) in the UD plies and the surface based cohesive contact at the interfaces between each plies. The element size in the drilling zone is defined as 260 μm which is equal to the thickness of a ply. 90,000 elements are used in the UD CFRP work piece. The drill is meshed using 3D, 3-node triangular facet rigid elements (R3D3). The mesh of the drill is refined with 200 μm elements at the drill tip. The drill is comprised of 20,000 elements. The FE model is shown in Fig. 1 (b).

2.1.2 Boundary Conditions and Loading

The boundary conditions of the drilling process are as follows. The work piece is fixed from the bottom surface. The bottom and top surfaces of the four fixture locations are also fixed in all displacement directions ($u_x=u_y=u_z=0$). At the beginning of the FE analysis the drill is located at the centre of the area to be drilled. The drill is restrained along its axis ($u_x=u_y=u_r=u_{r_x}=u_{r_y}=0$) so that the tool can only move along the cutting direction. The drill bit has a rotational velocity and a feed rate as process parameters. The heat generation is ignored since high amount of coolant has been used in the experiments to keep the temperature close to the room temperature.

In order to investigate the effect of cutting parameters on drilling, finite element analysis has been performed at the combinations of 4 cutting speeds and 4 feed rates. The parameters are given in the Table 1.

2.1.3 Constitutive Material Models

Inter laminar damage, delamination, is one of the predominant defects in a composite structure. Lack of reinforcement in thickness direction and weak inter laminar shear strengths are the main reasons of delamination. Delamination can cause a significant reduction, particularly in the compressive load capacity of the structure. The fracture process of composite laminates requires both inter laminar and intra laminar damage mechanisms. Therefore, UD laminated composite work piece is comprised of stacked plies with specified fibre orientations and interfaces between these plies. In the following subsections, material models of different components of the mesoscale FE model, namely plies and interfaces, will be explained.

Constitutive Material Model of Unidirectional Fibre Reinforced Plies: Each individual oriented UD-CFRP plies are modelled as linear elastic material with orthotropic behaviour.

Table 1 Cutting parameters used in the drilling of Hexcel M21 T700 GC

Cutting speed (m/min) [Spindle Speed (rpm)]	Feed (mm/min)
75.4, 113.1, 150.8, 226.19 [3000, 4500, 6000, 9000]	355, 457, 584, 685

Then fibre orientations are specified individually. The stress–strain relations for the in-plane components of the stress and strain can be formulised as below.

$$[\sigma] = [C][\varepsilon] \tag{1}$$

$$\begin{bmatrix} \sigma_{11} \\ \sigma_{22} \\ \tau_{12} \end{bmatrix} = \begin{bmatrix} \frac{E_1}{1 - \nu_{12}\nu_{21}} & \frac{\nu_{21}E_1}{1 - \nu_{12}\nu_{21}} & 0 \\ \frac{\nu_{12}E_2}{1 - \nu_{12}\nu_{21}} & \frac{E_2}{1 - \nu_{12}\nu_{21}} & 0 \\ 0 & 0 & G_{12} \end{bmatrix} \begin{bmatrix} \varepsilon_{11} \\ \varepsilon_{22} \\ \gamma_{12} \end{bmatrix} \tag{2}$$

where 11 and 22 denote local longitudinal and transverse directions respectively. The material properties of UD-CFRP are given in Table 2.

Constitutive Material Model of Interfaces: Traction-separation based cohesive contact has been used to model material discontinuities. Surface based cohesive contact is defined between the UD plies where delamination is expected to occur in the CFC work piece. The traction-separation cohesive material model assumes a linear elastic behaviour for the interfaces. Uncoupled elastic stress–strain relations of such interfaces can be explained as below regarding to the element directions.

$$[\sigma] = [K][\varepsilon] \tag{3}$$

$$\begin{bmatrix} \sigma_n \\ \sigma_s \\ \sigma_t \end{bmatrix} = \begin{bmatrix} K_{nn} & 0 & 0 \\ 0 & K_{ss} & 0 \\ 0 & 0 & K_{tt} \end{bmatrix} \begin{bmatrix} \varepsilon_n \\ \varepsilon_s \\ \varepsilon_t \end{bmatrix} \tag{4}$$

where n denotes normal direction; s and t denote shear directions.

Constitutive Damage Model of Unidirectional Fibre Reinforced Plies: There are many proposed failure theories to predict the onset of failures and their progression in composites. Most of the failure criteria are based on the stress state of a lamina. It should be noted that the failure criteria are intended to predict the macroscopic failures, therefore microscopic damages such as debonding of a fibre from the matrix cannot be determined. Failure criteria of composite materials can be divided into two main groups, namely: independent failure criteria and polynomial failure criteria.

The maximum stress criteria and the maximum strain criteria are the examples of the independent failure criteria. In these criteria, there isn't any dependence between the stress/strain components. This means a component in the longitudinal direction does not affect the

Table 2 Material properties of Hexcel M21 T700 GC [26, 27]

E_1 (MPa)	$E_2=E_3$ (MPa)	$G_{12}=G_{13}$ (MPa)	G_{23} (MPa)	$\nu_{12}=\nu_{13}$	ν_{23}	d (kg/m ³)
112000	8200	4500	3000	0.3	0.4	1580

component in the transverse direction or stacking direction. Polynomial maximum stress criterion, Polynomial maximum strain criterion, Tsai [18], Tsai-Hill [19], Tsai-Azzi [20], Hoffman [21], Tsai-Wu [22] and Hashin [23, 24] criteria are the examples of the polynomial failure criteria. In all these criteria, there is dependence between the components in each direction. However, in all above only Hashin’s criteria can predict the initial failure regarding to the mode of failure namely fibre and matrix.

Due to the fact that fibre composites consist of mechanically dissimilar phases such as stiff elastic brittle fibres and soft matrix, the failure occurs significantly distinct for each constituent. Fibres may rupture in tension or buckle in compression and the matrix may fail due to the transferred load from the fibres. Moreover, failure mechanisms are different in tension and compression in each direction. In this study, the Hashin’s criteria were chosen because they can distinguish between different failure modes and are compatible with finite element analysis.

Typical stress-displacement behaviour of such material is shown in Fig. 2 (a). The positive slope of the stress-displacement graph presents the material behaviour prior to damage initiation; the negative slope of the graph displays the damage evolution after damage initiation in any model.

The material properties for the damage model of M21 are given in the Table 3.

Damage Initiation: The damage initiation criteria for FRP composites are based on Hashin’s theory [23, 24]. The initiation behaviour is also assumed to be orthotropic and the initiation criteria consider four different damage initiation mechanisms namely fibre tension, fibre compression, matrix tension, and matrix compression. These four initiation criterion are computed according to the Eqs. 5, 6, 7 and 8.

Fibre Tension ($\sigma_{11} \geq 0$)

$$F_f^T = \left(\frac{\sigma_{11}}{\sigma_{11}^{f,t}} \right)^2 + \psi \left(\frac{\tau_{12}}{\tau_{12}^f} \right)^2 \tag{5}$$

Fibre Compression ($\sigma_{11} \leq 0$)

$$F_f^C = \left(\frac{\sigma_{11}}{\sigma_{11}^{f,c}} \right)^2 \tag{6}$$

Matrix Tension ($\sigma_{22} \geq 0$)

$$F_m^T = \left(\frac{\sigma_{22}}{\sigma_{22}^{m,t}} \right)^2 + \left(\frac{\tau_{12}}{\tau_{12}^f} \right)^2 \tag{7}$$

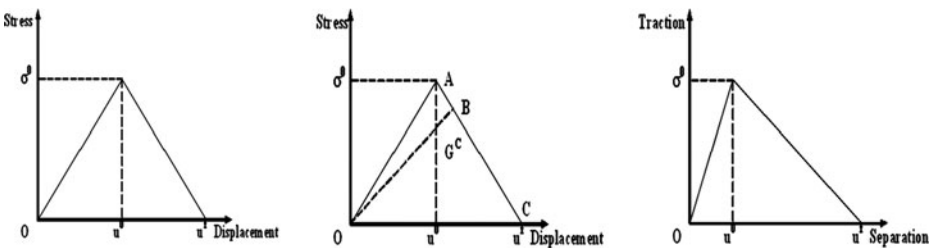


Fig. 2 a Equivalent stress-displacement. b Linear damage evolution. c Traction-separation behaviour of a cohesive zone

Table 3 Properties of damage model of Hexcel M21 T700 GC [15, 26]

$\sigma_1^{f,t}$ (MPa)	$\sigma_1^{f,c}$ (MPa)	$\sigma_2^{f,t}$ (MPa)	$\sigma_2^{f,c}$ (MPa)	τ_{12}^f (MPa)
1900	1000	84	250	110

Matrix Compression ($\sigma_{22} \leq 0$)

$$F_m^C = \left(\frac{\sigma_{22}}{2\tau_{12}^f} \right)^2 + \left[\left(\frac{\sigma_{22}^{f,c}}{2\tau_{12}^f} \right)^2 - 1 \right] \frac{\sigma_{22}}{\sigma_{22}^{f,c}} + \left(\frac{\tau_{12}}{\tau_{12}^f} \right)^2 \tag{8}$$

where m and f denote matrix and fibre; C and T denote compression and tension respectively.

Damage Evolution: When the Hashin’s criteria have been fulfilled in any mode, damage has initiated and evolution has started in that specific mode. The damage operator becomes significant in the criteria for damage initiation of other modes. The effective stress can be computed by Eq. 9.

$$\bar{\sigma} = C_d \varepsilon \tag{9}$$

$$C_d = \frac{1}{D} \begin{bmatrix} (1 - d_f)E_1 & (1 - d_f)(1 - d_m)v_{21}E_1 & 0 \\ (1 - d_f)(1 - d_m)v_{12}E_2 & (1 - d_m)E_2 & 0 \\ 0 & 0 & (1 - d_s)GD \end{bmatrix} \tag{10}$$

$$D = 1 - (1 - d_f)(1 - d_m)v_{12}v_{21} \tag{11}$$

The damage variables of stiffness matrix for a particular mode can be defined as defined in Eq. 12

$$\begin{aligned} d_f &= \begin{cases} d_f^T & \text{if } \bar{\sigma}_{11} \geq 0 \\ d_f^C & \text{if } \bar{\sigma}_{11} \leq 0 \end{cases} \\ d_m &= \begin{cases} d_m^T & \text{if } \bar{\sigma}_{22} \geq 0 \\ d_m^C & \text{if } \bar{\sigma}_{22} \leq 0 \end{cases} \\ d_s &= 1 - (1 - d_f)(1 - d_m) \end{aligned} \tag{12}$$

where f, m, s denote fiber, matrix and shear; C and T denote compression and tension respectively.

After the damage initiation ($\delta_{eq} \geq \delta_{eq}^0$), the damage variable can be calculated from the following expression for each damage mode.

$$d = \frac{u_{eq}^f (u_{eq} - u_{eq}^0)}{u_{eq} (u_{eq}^f - u_{eq}^0)} \tag{13}$$

The energy dissipation (G^C) of any mode due to failure corresponds to the area of the triangle OAC in Fig. 2 (b) and the failure displacement can be calculated from Eq. 14.

$$u^f = 2G^C / \sigma_{eq}^0 \tag{14}$$

Constitutive Damage Model of Interface: In meso-scale modelling, the composite laminate is designed as an assembly of two components, namely the fibre reinforced plies and the interfaces or cohesive zone. The application of these interfaces allows modelling of delamination of the plies. In this approach, the interface is considered as an independent material which joins the two plies of the laminates and has its own constitutive law. The material properties for the damage model of cohesive interfaces are given in the Table 4.

Damage Initiation: The traction-separation cohesive model assumes a linear elastic behaviour followed by the initiation and evolution of damage. Once damage has initiated, gradual degradation of the interface can occur according to the evolution law. A typical traction-separation response with a failure mechanism is shown in Fig. 2 (c). The positive slope of the stress-displacement graph presents the material behaviour prior to damage initiation; the negative slope of the graph displays the damage evolution after damage initiation.

In this study damage initiation is predicted with the use of quadratic nominal stress criterion which is represented as below.

$$\left\{ \frac{\langle \sigma_n \rangle}{\sigma_n^0} \right\}^2 + \left\{ \frac{\sigma_s}{\sigma_s^0} \right\}^2 + \left\{ \frac{\sigma_t}{\sigma_t^0} \right\}^2 = 1 \tag{15}$$

Damage Evolution: The damage evolution law describes the rate at which the material stiffness is degraded once the damage initiation criterion is reached. The damage operator D represents the overall damage in the material and the stress components of the cohesive model are calculated according to Eq. 16.

$$\begin{aligned} \bar{\sigma}_n &= \begin{cases} (1 - D)\sigma_n, & \sigma_n \geq 0 \\ \sigma_n & \text{otherwise} \end{cases} \\ \bar{\sigma}_s &= (1 - D)\sigma_s, \\ \bar{\sigma}_t &= (1 - D)\sigma_t, \end{aligned} \tag{16}$$

The effective displacement is defined as below [25]

$$u_m = \sqrt{\langle u_n \rangle^2 + u_s^2 + u_t^2} \tag{17}$$

Table 4 Properties of damage model of cohesive [15, 28]

σ_{nn}^f (MPa)	σ_{ss}^f (MPa)	σ_{tt}^f (MPa)	G_{nn}^C (N/mm)	G_{ss}^C (N/mm)	G_{tt}^C (N/mm)
60	110	110	0.33	1.209	1.209

The second component of the damage evolution is the specification of the nature of the evolution of the damage. This can be done by using energy or displacement criterion and either defining as linear, exponential softening law or as a tabular function. In this study, energy criterion has been used with a linear softening law, which can be expressed as below.

$$D = \frac{u_m^f (u_m - u_m^0)}{u_m (u_m^f - u_m^0)} \tag{18}$$

where $u_m^f = 2G^C / \sigma^0$

The mixed mode conditions is applied by using the power law criterion states that failure under mixed-mode and given as

$$\left\{ \frac{G_n}{G_n^C} \right\}^\alpha + \left\{ \frac{G_s}{G_s^C} \right\}^\alpha + \left\{ \frac{G_t}{G_t^C} \right\}^\alpha = 1 \tag{19}$$

when the Eqs. 2, 3, 4, 5, 6, 7, 8, 9, 10, 11, 12, 13, 14, 15, 16, 17, 18, 19 and 20 is satisfied, the mixed-mode fracture energy is equal to

$$G^C = G_n + G_s + G_t \tag{20}$$

Tool Material: Cutting tools materials have higher strength and are harder comparing to the materials to be machined what brings brittle characteristics to the cutting tool. As explained in the section above, the drill is assumed fully elastic material in order to calculate mass and inertia of the 3D complex tool geometry in the FE model. Then it is modelled as a rigid body. Tungsten carbide is used as drill material. The properties of the drill are given in Table 5.

2.1.4 Contact Modelling

The contact model controls the interaction between the surfaces of the tool and work piece material, namely friction and master–slave relationship. Based on Coulomb friction model, which is given in the Eq. 21, it is assumed that the frictional stresses, τ_n , on the drill have been considered proportional to the normal stresses, σ_n , with a constant friction coefficient, μ .

$$\tau_n = \mu \sigma_n \tag{21}$$

In this present study, the interaction between the work piece and the tool is modelled by using surface-surface kinematic contact available in ABAQUS/Explicit. The surface of the tool is set to be the master object and the surface of the work piece is the slave object. This means that the work piece will deform according to the motion of the tool and the elements in the work piece cannot penetrate into the tool. The coefficient of friction is set equal to 0.15 what was obtained from pin on disk tests.

Table 5 The properties of Tungsten Carbide [29]

d (kg/m ³)	E (GPa)	ν
14500	580	0.22

2.2 Digital Image Analysis

Several techniques can be employed to analyze delamination after drilling composites, such as optical microscopy, CT-Scan, and digital photography. In the present work, the digital image analysis of the damaged area is used to assess the extent of delamination at the hole entrance.

A digital image is considered as a matrix where each element of columns and rows identify one point of the image known as pixel. Pixels are corresponded to the lumens intensity. The digital image processing can produce satisfactory results with quantitative outputs.

Figure 3 (a) shows typical delamination damage in the composite material. The delamination factor has been widely used to characterize the level of damage on the work material at the entrance and exit of the drill. The delamination factor (F_D) is generally calculated from the ratio of the maximum diameter (D_{max}) of the delamination zone to the drill diameter (D_{nom}), as indicated in Eq. 22. Alternatively, delamination factor (F_A) can be calculated from the ratio of the delaminated area (A_{damage}) to the nominal hole area (A_{nom}) as given in Eq. 23.

$$F_D = \frac{D_{max}}{D_{nom}} \quad (22)$$

$$F_A = \frac{A_{damage}}{A_{nom}} \quad (23)$$

The delamination factors are obtained through the digital image analysis. Figure 3 (b) illustrates the flow diagram of the digital image analysis procedure. The algorithm has been developed in Matlab environment. The image from optical microscope is loaded to the software. In order to obtain an image with acceptable quality, a series of parameters must be appropriately selected. First threshold filter is applied to the image then the noise is suppressed in order to make a clear image. After the application of edge detection module, the image is divided into areas to enable obtaining quantitative data on the image. Finally, the maximum diameter and damaged area are measured and delamination factors are calculated.

2.3 Experiments

The carbon fibre reinforced composite work piece was mounted on a dynamometer on a table of the milling machine. The thrust force and torque during machining were measured

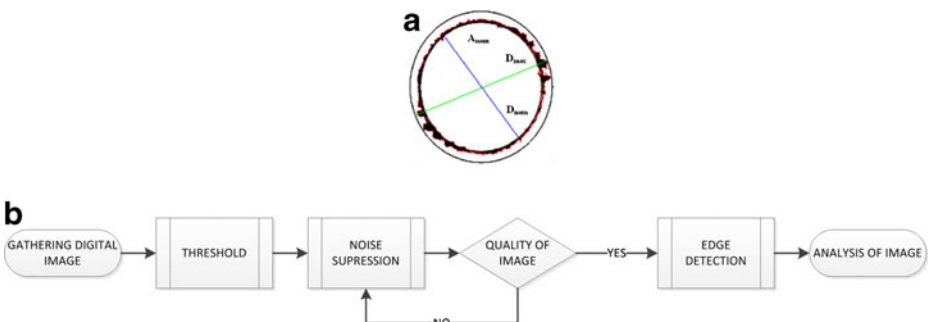


Fig. 3 **a** Delamination. **b** The flow diagram of the digital image analysis

using the dynamometer (Kistler 9255B). Dynamometer is charged and the signals are collected by a data acquisition system which includes a multi channel charge amplifier (Model 5017) and Kistler Dynoware software.

Drilling tests have been performed using 8 mm diameter Sandvik CoroDrill Delta-C R846 solid carbide drills which are 3 μm TiAlN coated tungsten carbide drills. The drilling trials were conducted using Mori Seiki SV-500 milling machine. All tests were carried out with the use of 5% emulsion of Hocut 795B cutting fluid. In all the tests the coolant pressure was 38 bar. Experiments were repeated 5 times and the results reported are all mean values.

The delamination was investigated. The delamination was observed by optical microscope and the extent of delamination was measured using developed algorithm in Matlab explained in the previous subsection.

3 Results and Discussion

3.1 Validation of the FE Model

In order to validate the FE model in the following the comparison of the experimental and simulated thrust force and torque in the drilling of UD-CFRP at 457 mm/min feed rate and 4500 rpm spindle speed (113 m/min cutting speed) is presented.

The drilling of a through hole consists of three stages. In the first phase drill penetrates into the work piece. In the second phase, in which the whole cutting edges are in contact with the work piece, a steady state torque and thrust is attained. Finally, in the third phase the drill point exits or breaks through the other side of the work piece. These three stages are clearly shown in Fig. 4 in both the experimental and simulation results.

Figure 4 (a) and (b) show the experimental and simulated thrust force and torque in the drilling of UD-CFRP at 457 mm/min feed rate and 4,500 rpm spindle speed (113 m/min cutting speed), respectively.

It was observed that the thrust force in the experimental trial was 230 N, whereas the FE model estimated 225 N. The experimentally measured torque was 0.29 N.m compared to the torque value predicted as 0.3 N.m by the FE simulation. This shows that the FE model estimated the thrust force and torque very accurately with 2.17% and 3.45% deviation from the test results, respectively. Similar comparisons between experimental and simulation results are performed for other process parameters and similar level of agreement was observed. This gave the confidence about the capability of the FE model in its prediction of the thrust forces and torque values. It should be noted that several factors could affect the accuracy of the simulation results. Amongst these are using more realistic friction model, improved damage model, inclusion of thermal and wear effect and also including the deformation of the drill. However each of these parameters would add to the computing resources required substantially. The developed model already requires four months for a full run on a workstation which has 32 Gb RAM and a processor with 8 core, each of them has 3.16 Ghz CPU.

3.2 Analysis of Thrust Force

Figure 5 (a) shows the effect of cutting parameters on the thrust force. The FE model estimated the thrust force between 145 and 352 N depending on the cutting parameters. The

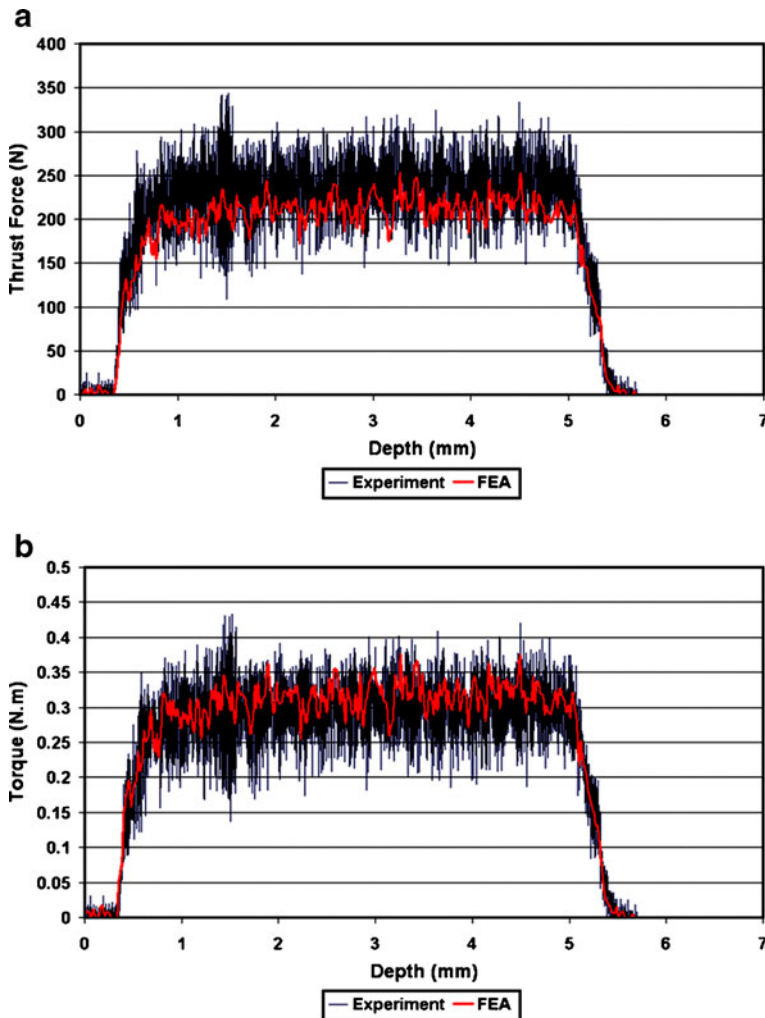


Fig. 4 Validation of FE model. **a** Thrust force. **b** Torque

results indicate that the drilling induced thrust force decreased with the increasing cutting speed. As it can be observed from Fig. 5 (a), the thrust force was the highest at the cutting speed of 75.4 m/min (3,000 rpm spindle speed) at various feed rates. In contrast, the minimum cutting speed was observed at 226.2 m/min cutting speed (9,000 rpm spindle speed). Comparing the thrust force between the simulations performed at different cutting speeds, 200% increase in the cutting speed led to a fall in the thrust force between 34.1% and 43.3% depending on the feed rate.

Figure 5 (a) also depicts the influence of the feed rate on the thrust force. In contrast to the correlation between the cutting speed and thrust force, it was observed that thrust force rose with the increasing feed rate. It was predicted that 93% higher feed rate caused an increase of the thrust force between 42.7% and 60% depending on the cutting speed.

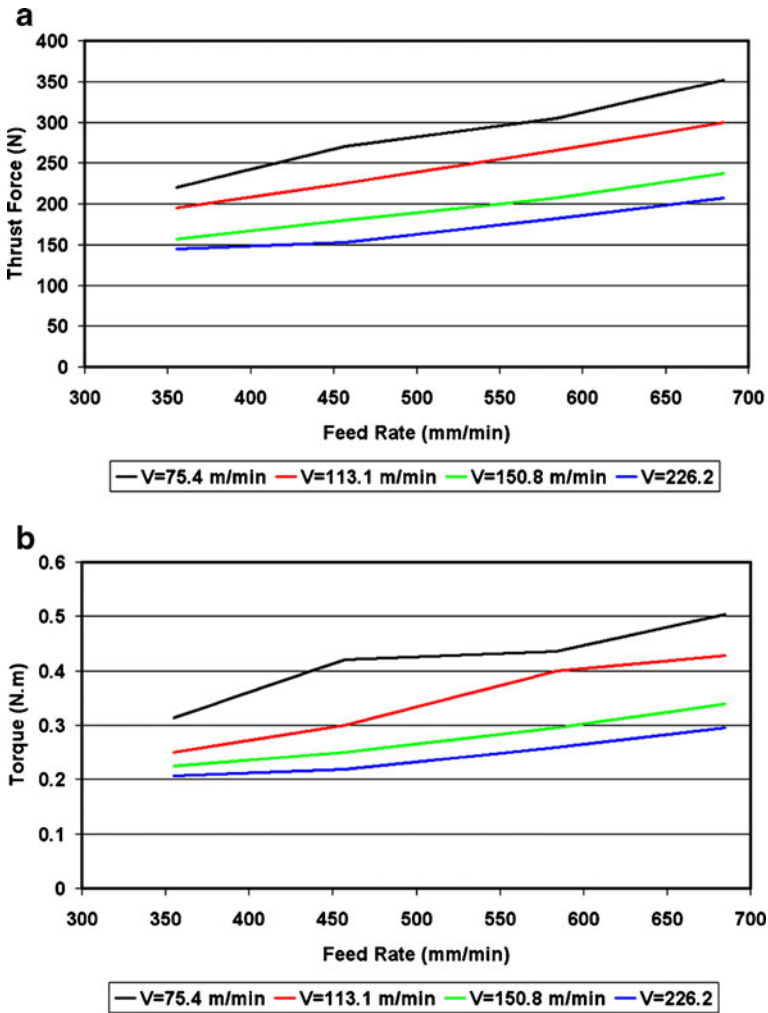


Fig. 5 Effects of cutting parameters on (a) Thrust force (b) Torque

3.3 Analysis of Torque

Figure 5 (b) shows the induced torque corresponding to different cutting parameters. The induced torque was estimated between 0.2 and 0.5 N.m in the FE analysis at different cutting process parameters.

Figure 5 (b) shows the effect of the cutting speed on the torque at four different feed rates. It was observed that the drilling induced torque has a tendency to decrease with the increasing cutting speed. As it is shown in the figure, the induced torque reaches maximum when the drilling is carried out at the minimum cutting speed whereas the minimum induced torque can be observed in the drilling performed at the maximum cutting speed. It can also be noticed that 200% increase in the cutting speed results in a fall between 34.1% and 47.96% in the torque in the FE analysis depending on the feed rate.

Figure 5 (b) also represents the influence of the feed rate on the torque at four different cutting speeds. Finite element analysis results show that the drilling induced torque rises with the increasing feed rate. Each different case indicates that the maximum induced torque occurs as the drilling is performed at the maximum feed rate in the test range. It was observed that when the drilling is performed at 93% increased feed rate, the torque is increased between 42.76% and 71.43% in FE analysis depending on the cutting speed.

3.4 Analysis of Stress in the Work Piece

The progressive damage and the stress distributions of the unidirectional carbon fibre reinforced laminated composite work piece during the drilling process are shown in the Fig. 6. As it can be observed from the images, stress is induced in the work piece as the drill touches the work piece material surface. As the drill moves into the material, the material goes under orthotropic linear elastic behaviour depending on the fibre orientation, consequently fails according to the damage model. When the elements fail, they are removed from the model.

Figure 7 shows the Hashin's Damage Criteria at the onset of the damage initiation in four different failure modes during the drilling of unidirectional carbon fibre laminated composite work piece.

Figures 7 (a) and (b) show the contour plots of the F_f^T and F_f^C respectively at the time of 0.4 s of drilling process. These parameters are defined in Eqs. 5 and 6 of methodology section. The areas of the work piece for which the values of F_f^T and F_f^C reach to 1, failure in that mode occurs. Comparison of Figs. 7 (a) and (b) indicates that the dominant mode of failure in fibre is compression. This result is expected since the compressive failure strength of the any ply in the fibre direction is significantly lower comparing to the tensile failure strength.

Figures 7 (c) and (d) show the contour plots of the F_m^T and F_m^C respectively at the time of 0.4 s of drilling process. These parameters are defined in Eqs. 7 and 8 of methodology section. The areas of the work piece for which the values of F_m^T and F_m^C reach to 1, failure in that mode occurs. Comparison of Figs. 7 (c) and (d) indicates that the dominant mode of failure in matrix is tension. The reason is that the tensile failure strength of a ply in the transverse direction is lower comparing to the compressive failure strength.

3.5 Analysis of Delamination

The features observed at the entrance of the drilled laminate are presented in Fig. 8. The figure shows the delamination obtained through the digital image processing. These delamination figures are used to evaluate the effects of process parameters on delamination after drilling CFRP. The figure indicates a typical brittle damage due to the abrasive fibres in the structure.

Figure 9 (a) shows both delamination factors (F_D and F_A) obtained under different cutting conditions after the drilling experiments. It can be seen that the delamination factor (F_A) relating to the damaged area provides generally smaller delamination factor compared to the conventional delamination factor (F_D). The conventional delamination factor is very much dependent on the local maximum damaged point on the image. It can also be noted that delamination increases with the feed rate and decreases with the cutting speed in the test region. When the cutting speed was increased 200%, the delamination decreased between 8.5% and 14% whereas the increase of the feed rate by 93% caused the reduction in the delamination between 4% and 9.5% depending on the process parameters.

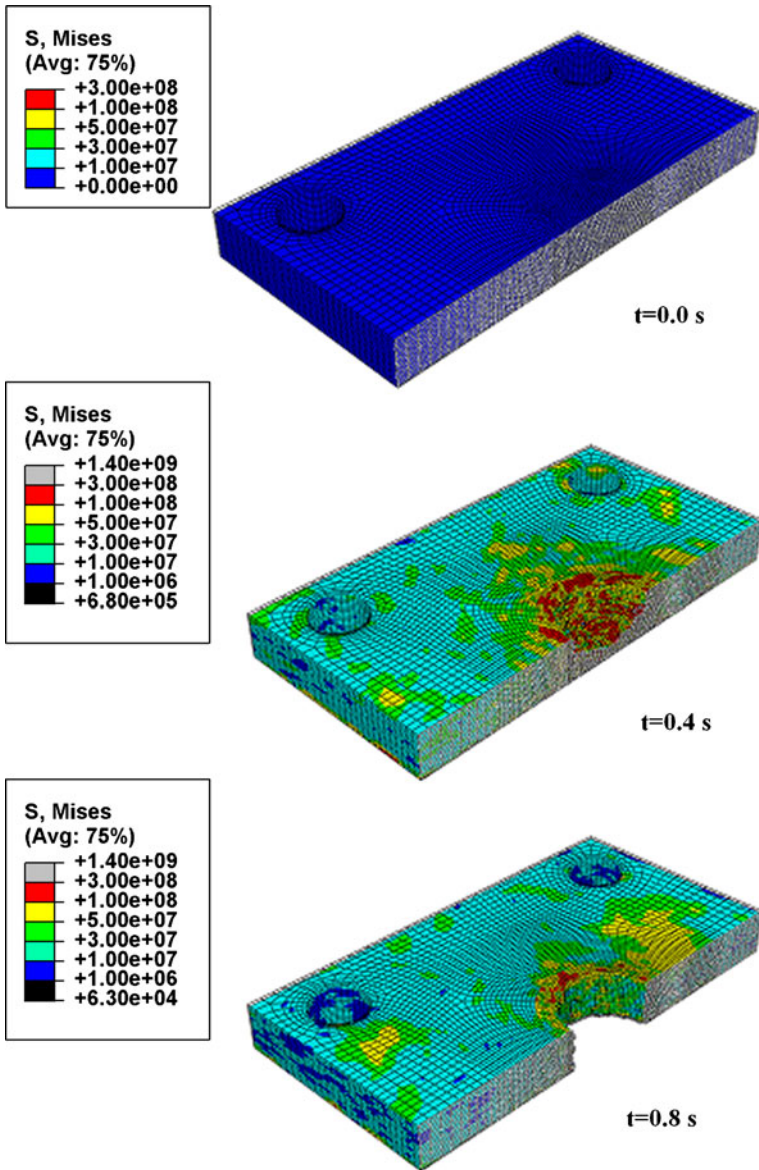


Fig. 6 Stress distributions in the UD-CFRP work piece ($S=4500$ rpm, $f=457$ mm/min)

Figure 9 (b) shows delamination factors (F_A) evaluated through the simulation results under different cutting conditions. It can be seen that the general trend of delamination factor (F_A) is similar to the experimental results, delamination increases with the feed rate and decreases with the cutting speed in the range simulated. When the cutting speed increased 200%, the delamination decreased between 9% and 12.3% whereas the increase of the feed rate by 93% resulted in the increase of the delamination between 13.7% and 21.8% depending on the process parameters. FE model overestimated the delamination between 7% and 28% depending on the cutting parameters. The FE model predicts more

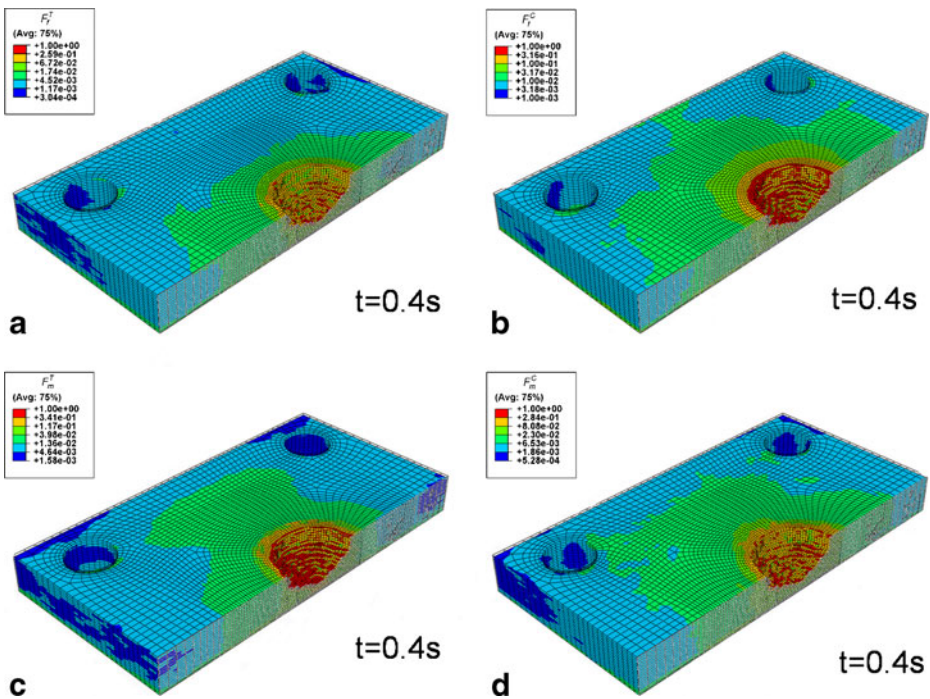


Fig. 7 Hashin's failure modes in the UD-CFRP Work Piece ($S=4,500$ rpm, $f=457$ mm/min). **a** Fibre tension mode. **b** Fibre compression mode. **c** Matrix tension mode. **d** Matrix compression mode

sensitivity to the feed rate. The difference between the experiments and simulation results becomes larger at higher feed rates. It should be mentioned that the trends predicted by the FE model is always in agreement with the experimental values for the delamination. In general in order to achieve very accurate results for prediction of delamination using simulation, extremely fine mesh and very good damage model are essential. However due to the complexity of the geometry and the process moving to very fine mesh would require huge computing resources. Limitation in the computing resources and computing time had restricted us in terms of the mesh refinement. Within the resources available the accuracy of the predictions of the delamination factors for different process parameters is acceptable.



Fig. 8 Digital image processing of delamination

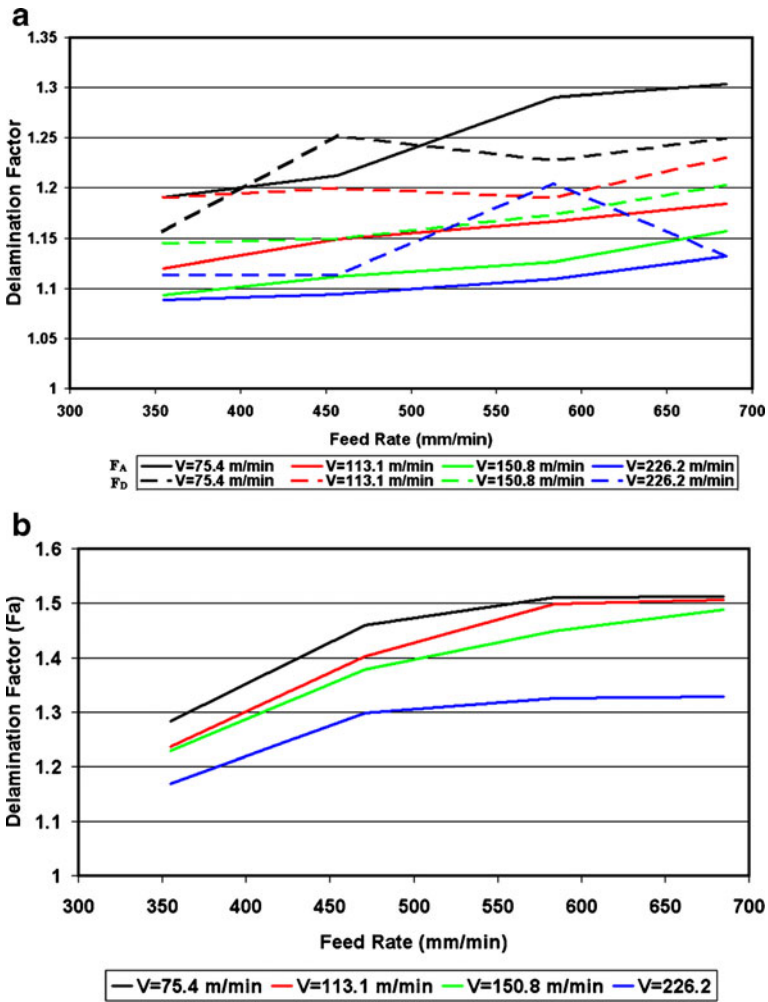


Fig. 9 Effects of cutting parameters on entrance delamination. a Experimental. b Finite element analysis

4 Conclusion

In this study, a mechanical Lagrangian finite element formulation is used to simulate the drilling process of unidirectional carbon fibre reinforced laminated composite material. The effects of cutting parameters, namely cutting speed and feed rate, on drilling are investigated by the proposed FE model. Experimental validation tests were performed; and the thrust force and torque were experimentally measured throughout the process. In addition to that delamination at the entrance of the holes was experimentally observed and digital analysis of the images was carried out. Delamination factors were identified.

The results show that cutting parameters have a significant influence on the stress, thrust force, torque and delamination. The thrust force is slightly underestimated whereas torque and delamination are overestimated. Results clearly show that the induced thrust force, torque and delamination increase with the feed rate and decrease with the cutting speed.

This study can justify that the finite element simulation technique is a feasible, accurate and parametric analysis method which can be used in the drilling process. For the future studies related to drilling process, a thermo-mechanical model is needed. Having an appropriate friction coefficient and an improved friction model for the different regimes of tool and work piece interfaces would also provide better predictions.

Acknowledgement Authors greatly acknowledge the provision of materials by Airbus and the access to the drilling facilities of the Advanced Machining Research Centre (AMRC) at University of Sheffield. The funding of the PhD scholarship of Mr. Ozden Isbilir supplied by the Ministry of National Education of the Republic of Turkey is highly appreciated.

References

- Hocheng, H., Tsao, C.C.: Effects of special drill bits on drilling-induced delamination of composite materials. *Int. J. Mach. Tool. Manufact.* **46**(12–13), 1403–1416 (2006)
- Koenig, W., Grass, P., Heintze, A., Okcu, F., Schmitz-Justin, C.: Developments in drilling, contouring composites containing Kevlar. *Prod. Eng.* **63**(8), 56–61 (1984)
- Hocheng, H., Tsao, C.C.: The path towards delamination-free drilling of composite materials. *J. Mater. Process Tech.* **167**(2–3), 251–264 (2005)
- Khashaba, U.A.: Delamination in drilling GFR-thermoset composites. *Compos. Struct.* **63**(3–4), 313–327 (2004)
- Abrate, S.: Machining of composite materials. In: Mallick, P.K. (ed.) *Composites Engineering Handbook*, pp. 777–809. Marcel Dekker, New York (1997)
- Persson, E., Eriksson, I., Zackrisson, L.: Effects of hole machining defects on strength and fatigue life of composite laminates. *Compos. Appl. Sci. Manuf.* **28**(2), 141–151 (1997)
- Persson, E., Eriksson, I., Hammersberg, P.: Propagation of hole machining defects in pin-loaded composite laminates. *J. Compos. Mater.* **31**(4), 383–408 (1997)
- Hocheng, H., Dharan, C.K.H.: Delamination during drilling in composite laminates. *J. Eng. Ind.* **112**, 236–239 (1990)
- Jain, S., Yang, D.C.H.: Effects of feed-rate and chisel edge on delamination in composites drilling. *Trans. ASME* **115**, 398–405 (1993)
- Lachaud, F., Piquet, R., Collombet, F., Surcin, L.: Drilling of composite structures. *Compos. Struct.* **52** (3–4), 511–516 (2001)
- Pyo Jung, J., Woo Kim, G., Yong Lee, K.: Critical thrust force at delamination propagation during drilling of angle-ply laminates. *Compos. Struct.* **68**(4), 391–397 (2005)
- Zhang, L.B., Wang, L.J., Liu, X.Y.: A mechanical model for predicting critical thrust forces in drilling composite laminates. *Proc. IME B J. Eng. Manufact.* **215**(2), 135–146 (2001)
- Arola, D., Ramulu, M.: Orthogonal cutting of fiber-reinforced composites: a finite element analysis. *Int. J. Mech. Sci.* **39**(5), 597–613 (1997)
- Zitoun, R., Collombet, F.: Numerical prediction of the thrust force responsible of delamination during the drilling of the long-fibre composite structures. *Compos. Appl. Sci. Manuf.* **38**(3), 858–866 (2007)
- Zitoun, R., Collombet, F., Lachaud, F., Piquet, R., Pasquet, P.: Experiment-calculation comparison of the cutting conditions representative of the long fiber composite drilling phase. *Compos. Sci. Tech.* **65**(3–4), 455–466 (2005)
- Durão, L.M.P., de Moura, M.F.S.F., Marques, A.T.: Numerical simulation of the drilling process on carbon/epoxy composite laminates. *Compos. Appl. Sci. Manuf.* **37**(9), 1325–1333 (2006)
- Durão, L.M.P., de Moura, M.F.S.F., Marques, A.T.: Numerical prediction of delamination onset in carbon/epoxy composites drilling. *Eng. Fract. Mech.* **75**(9), 2767–2778 (2008)
- Tsai, S.W.: Strength theories of filamentary structures. In: Schwartz, R.T., Schwartz, H.S. (eds.) *Fundamental Aspects of Fiber Reinforced Plastic Composites*, pp. 3–11. Wiley, New York (1968)
- Hill, R.: *The Mathematical Theory of Plasticity*. Oxford University Press, London (1950)
- Tsai, S.W., Azzi, V.D.: Strength of laminated composite materials. *AIAA* **4**(2), 296–301 (1966)
- Hoffman, O.: The brittle strength of orthotropic materials. *J. Compos. Mater.* **1**(2), 200–206 (1967). doi:10.1177/002199836700100210

22. Tsai, S.W., Wu, E.M.: A general theory of strength for anisotropic materials. *J. Compos. Mater.* **5**(1), 58–80 (1971). doi:10.1177/002199837100500106
23. Hashin, Z.: Failure criteria for unidirectional fiber composites. *J. Appl. Mech.* **47**(2), 329–334 (1980)
24. Hashin, Z., Rotem, A.: Fatigue failure criterion for fiber reinforced materials. *J. Compos. Mater.* **7**, 448–464 (1973)
25. Camanho, P.P., Davila, C.G.: Mixed-mode decohesion finite elements for the simulation of delamination in composite materials. In: NASA (ed.). pp. 1–37. (2002)
26. Hexcel Product Datasheet. http://www.hexcel.com/NR/rdonlyres/A4AE89BC-0EA6-473A-A3CA-F2F98C13D033/0/HexPly_M21_eu.pdf. Accessed 10/01/2009
27. Irisarri, F.-X., Bassir, D.H., Carrere, N., Maire, J.-F.: Multiobjective stacking sequence optimization for laminated composite structures. *Compos. Sci. Tech.* **69**(7–8), 983–990 (2009)
28. Bertolini, J., Castanié, B., Barrau, J.-J., Navarro, J.-P.: Multi-level experimental and numerical analysis of composite stiffener debonding. Part 1: Non-specific specimen level. *Compos. Struct.* **90**(4), 381–391 (2009)
29. ASM Handbook, Volume 16: Machining, vol. 16. ASM Handbook. ASM International, (1995)